# Efficient Uncertainty Quantification of Wharf Structures under Seismic Scenarios using Gaussian Process Surrogate Model

Lei Su[1], Hua-Ping Wan[2*], You Dong[2], Dan M. Frangopol[3], Xian-Zhang Ling[1]

[1]*School of Civil Engineering, Qingdao University of Technology, Qingdao, China*

[2]*Department of Civil and Environmental Engineering, The Hong Kong Polytechnic University, Kowloon, Hong Kong*

[3]*Department of Civil and Environmental Engineering, Lehigh University, Bethlehem, PA, USA*

## Abstract

The scenario-based seismic assessment approach is illustrated within a large-scale pile-supported wharf structure (PSWS). As nonlinear seismic response analysis is computationally expensive, a novel and efficient method is developed to improve and update the traditional simulation methods (e.g., Monte Carlo simulation (MCS)). Herein, the Gaussian Process (GP) surrogate model is proposed to replace the time-consuming FE model of PSWS, which makes the quantification of uncertainty in seismic response of a large-scale PSWS resulting from structural parameter uncertainty more computationally-efficient. The feasibility of the proposed GP surrogate model-based approach in uncertainty quantification of seismic response of a large-scale structural system under a given seismic scenario is verified and compared by using MCS.

**Keywords:** Pile-supported wharf structure; Uncertainty; Scenario-based seismic assessment; Finite element; Surrogate model; Sobol sequence

*Corresponding author.
*E-mail address*: slqd@qut.edu.cn (L. Su); huaping.wan@polyu.edu.hk (H.-P. Wan); you.dong@polyu.edu.hk (Y. Dong); dan.frangopol@lehigh.edu (D. M. Frangopol); ling_xianzhang@163.com (X.-Z. Ling).

## 1 Introduction

Pile-supported wharf are structures located on the shore of a harbor or on the bank of a river and canal, where ships may dock to load and unload cargo or travelers. A wharf structure is essential to a port transportation system and plays an important role in protecting capital investments and promoting the regional and national prosperity. Typically, a wharf structure includes one or more berths, and may also include pile foundation, deck, and other necessary facilities for handling the container. A pile-supported wharf structure (PSWS) is susceptible to severe damage during strong earthquakes, as the seismic-induced sand liquefaction and lateral deformation of the offshore slope would usually result in excessive axial force and bending moment around the pile-deck connection [1, 2]. The seismic damage to PSWS has been reported in many recent seismic cases [3-5], such as the 1995 Hyogoken-Nanbu earthquake [4] and the 2010 Haiti earthquake [5]. To mitigate the seismic-induced damage of a PSWS, it is crucial to understand and predict its seismic performance during earthquakes.

However, accurate characterization of seismic performance of a PSWS is not an easy task. During the last two decades, tests, including either full-scale or centrifuge test and in-field experimental test, have been conducted to study the seismic behavior of PSWS [6-8]. Numerical simulation has also drawn considerable attention of engineers to investigate the seismic behavior of PSWS owing to its low cost and modeling generality. Some studies have been conducted to investigate the seismic performance assessment of PSWS based on numerical analysis [9-14]. In general, the representative numerical model of PSWS usually consists of a lot of physical and mechanical properties, including compressive strength of concrete, soil-pile interface stiffness, shear strength, shear modulus, and friction angle of soil, yield strength and elastic modulus of steel among others.

Most studies considered structural properties to be deterministic. As such, the

subsequent nonlinear seismic response analysis is carried out in a deterministic manner. In practice, the geometric and material properties (such as, soil, steel, and concrete) are random [15, 16, 17]. Thus, the effect of parameter uncertainty on seismic responses of PSWS should be taken into account in order to ensure accurate characterization of the seismic behavior. The significance of uncertainty quantification of seismic performance has been increasingly recognized, and, in response, a large volume of work has been done on this topic. In the literature, most studies focus on buildings [17-24] and bridges [25-35], while little has been devoted to PSWS [36, 37]. Specifically, Nour et al [36] and Mirfattah and Lai [37] assessed the seismic responses of the wharf considering the random soil properties beyond MCS. Heidary-Torkamani et al. [38, 39] also studied the probabilistic seismic analysis of wharf structure with uncertain parameters, but they focused on sensitivity analysis to find the relative importance of uncertain structural parameters to seismic responses.

Due to its robustness, generality, and ease of use, MCS has wide applications in uncertainty quantification. However, it requires a large number of model runs and is prohibitively computationally expensive as its convergence rate is very low, requiring a huge number of model realizations to achieve well converged estimates. As a result, MCS may become impractical for probabilistic seismic analysis of large-scale and complex structural systems. Several strategies are possible to improve the computational efficiency of MCS in the uncertainty quantification process. One attempt aims to reduce the sample size by adopting more efficient sampling techniques, such as Latin hypercube sampling [19-23, 26-31]. Another alternative is to replace the time-consuming FE model by a surrogate model (also termed as response surface model, metamodel, and emulator), which is a simplified and even explicit mathematical model used to map the relationship between the uncertain structural parameters and the target seismic response [17].

In this study, a Gaussian Process (GP) surrogate model is developed to assess the

probabilistic seismic performance of PSWS and improve the computational efficiency considering the uncertainties associated with structural parameters. To the best knowledge of the authors, the GP surrogate model has not been incorporated within the probabilistic seismic performance of wharf structures. The easy-to-use and fast-to-run GP surrogate model is adopted to substitute the computationally demanding model solver of PSWS. Subsequently, uncertainty quantification of seismic response is carried out within the framework of GP surrogate model, and the computationally expensive nonlinear seismic response analysis can be avoided. The most attractive benefit associated with GP surrogate model is that the complex high-dimensional integrals related to computations of both the mean and variance of seismic responses can be decomposed into simple one-dimensional integrals. Under this setting, quantification of the uncertainty in model responses resulting from random input parameters can be achieved in an analytical manner. The feasibility of the developed GP surrogate model-based method in quantification of uncertainty in seismic response propagated from structural parameter uncertainty is demonstrated through a large-scale and complex wharf structure.

## 2 GP surrogate model-based uncertainty quantification of seismic performance

### 2.1 Sobol sequence sampling

To build a reliable and accurate GP surrogate model for uncertainty quantification of seismic performance, a suitable design of experiments (DOE) method is needed. The selected DOE method should allow for generating sample points that provide maximum information about the behavior of the original physical system. In general, since the physical models tend to be highly complex and are not well-understood in advance, the space-filling DOE method, which does not require knowledge about the underlying model, may be preferred [40]. In this study, Sobol sequence sampling [41], which is a well-known quasi-random low-discrepancy sequence, has good coverage of parameter design space. As such, Sobol sequence sampling is

utilized to prepare training data for construction of GP surrogate model.

The Sobol sequence is a quasi-random low-discrepancy sequence, which exclusively uses the smallest prime number 2 as the base to form successively finer uniform partitions of the unit interval, and then reorder the coordinates in each dimension. Using base 2 not only gives high uniformity in high dimensions, but also has computational advantages through bit-level. To create the $n$-th point of Sobol sequence, consider that integer $n$ is written in radix-2 notation as

$$n = (\cdots n_3 n_2 n_1)_2 \tag{1}$$

The irreducible primitive polynomial whose coefficients are either 0 or 1 is introduced to Sobol points

$$p_i(x) = x^{s_i} + a_{1,i}x^{s_i-1} + a_{2,i}x^{s_i-2} + \cdots + a_{s_i-1,i}x + 1 \tag{2}$$

where $p_i(x)$ is the primitive polynomial of the $i$-th dimension, $s_i$ represents the degree of the primitive polynomial, The primitive polynomial coefficients $\{a_{1,i}, a_{2,i}, \cdots, a_{s_i-1,i}\}$ chosen from $\{0,1\}$ are used to define a sequence of positive integers $\{m_{1,i}, m_{2,i}, \cdots, m_{s_i,i}\}$ by the recurrence relation

$$m_{k,i} = 2a_{1,i}m_{k-1,i} \oplus 2^2 a_{2,i}m_{k-2,i} \oplus \cdots \oplus 2^{s_i-1}a_{s_i-1,i}m_{k-s_i+1,i} \oplus 2^{s_i}a_{s_i,i}m_{k-s_i,i} \oplus m_{k-s_i,i} \tag{3}$$

where $\oplus$ is the bit-by-bit exclusive-or operation, and $m_{k,i}(k = 1,2,\ldots,s_i)$ is an odd integer less than $2^k$. A set of direction numbers defined as a binary fraction of $m_{k,i}$ can be obtained from

$$v_{k,i} = \frac{m_{k,i}}{2^k} \tag{4}$$

The Sobol sequence is created from the following recurrence formula

$$x_{n,i} = n_1 v_{1,i} \oplus n_2 v_{2,i} \oplus n_3 v_{3,i} \cdots \tag{5}$$

In practice, the Gray code algorithm is employed to generate Sobol sequence [42]. Using the properties of Gray code, the subsequent Sobol points can be created recursively based on the preceding ones as follows

$$x_{k+1,i} = x_{k,i} \oplus v_{c_k,i} \tag{6}$$

where the superscript $c_k$ denotes the index of the rightmost zero bit in the binary representation of integrate $k$. A small demonstration of Sobol sequence generation using Gray code can be found in [43].

### 2.2 Modeling of seismic performance by GP

Nonlinear seismic response analysis of PSWS is computationally demanding, so the assessment of seismic performance is extremely time-consuming. In this paper, the surrogate modeling technique is adopted to solve the issue of high computational cost associated with the uncertainty quantification of seismic response. Specifically, a surrogate model is used to map the relationship between the structural parameters and the seismic responses; and then quantification of the uncertainty in the seismic responses propagated from parameter uncertainty is conducted within the framework of the reduced-order surrogate model. The GP surrogate model is used herein owe to its nonparametric and probabilistic features that enable it to maintain the benefits of the high modeling flexibility, great expressive power, and estimation of prediction uncertainty.

The definition of GP is that any infinite subset of the function outputs is assumed to have a joint multivariate Gaussian distribution [44]. GP surrogate model, usually called Bayesian emulator that is fully specified by the mean function and covariance function, is used to characterize the input-output relationship of PSWS. Accordingly, the seismic response of the PSWS can be expressed as

$$s(\mathbf{x}) \sim \mathrm{N}\left(M(\mathbf{x}), C(\mathbf{x},\mathbf{x}')\right) \tag{7}$$

where $\mathbf{x} = \{x_1, x_2, \ldots, x_d\}$ is $d$-dimensional parameter vector; $s$ is the seismic response of PSWS; $M(\bullet)$ is the mean function; and $C(\bullet,\bullet)$ is the covariance function. The mean function is in general set to be zero. On the other hand, the squared exponential covariance function is adopted. This is commonly used in engineering literature. The squared

exponential covariance function is [44]

$$C(\mathbf{x},\mathbf{x}') = \eta^2 \exp\left[-\frac{1}{2}\sum_{k=1}^{d}\left(\frac{x_k - x_k'}{\ell_k}\right)^2\right] \tag{8}$$

where $\eta^2$ is the signal variance and $\ell_k$ is the characteristic length scale.

To build the surrogate model $s(\mathbf{x})$, a small set of input and output data, called training data, generated from nonlinear seismic response analysis of PSWS is needed. The training dataset $\mathrm{D} = [\mathbf{X}, \mathbf{S}]$ consists of $n$ pairs of vector parameter sample and scalar output, in which $\mathbf{X} = \{\mathbf{x}_1, \mathbf{x}_2, \ldots, \mathbf{x}_n\}$ is the parameter index and $\mathbf{S} = \{s_1, s_2, \ldots, s_n\}$ is the seismic vector response. The task is to predict the seismic response $s_*$ at an untried point $\mathbf{x}_*$. Employing the postulation of Gaussian prior over model outputs, the following equations hold

$$p(\mathbf{S}) = \mathrm{N}\left(\mathbf{0}, C(\mathbf{X},\mathbf{X})\right) \tag{9}$$

$$p(\mathbf{S}, s_*) = \mathrm{N}\left(\begin{bmatrix}\mathbf{0}\\ 0\end{bmatrix}, \begin{bmatrix}C(\mathbf{X},\mathbf{X}) & C(\mathbf{X},\mathbf{x}_*)\\ C(\mathbf{x}_*,\mathbf{X}) & C(\mathbf{x}_*,\mathbf{x}_*)\end{bmatrix}\right). \tag{10}$$

Applying the Bayes' theorem, the posterior distribution of $s_*$ is

$$p(s_*) = \frac{p(\mathbf{S}, s_*)}{p(\mathbf{S})}. \tag{11}$$

Since the terms of Equation (11) have a Gaussian form, the posterior distribution over predicted outputs after integration is also Gaussian and can be expressed as

$$p(s_*) = \mathrm{N}\left(\mu_{s_*}, \sigma_{s_*}^2\right) \tag{12}$$

with the mean and the variance given by

$$\mu_{s_*} = \boldsymbol{\alpha}^{\cdot} \mathbf{C}_* \tag{13}$$

$$\sigma_{s_*}^2 = \tilde{C} - \mathbf{C}_*^{\cdot} \mathbf{C}^{-1} \mathbf{C}_* \tag{14}$$

where $\mathbf{C}_* = C(\mathbf{x}_*, \mathbf{X})$; $\mathbf{C} = C(\mathbf{X},\mathbf{X})$; and $\boldsymbol{\alpha} = \mathbf{C}^{-1}\mathbf{S}$.

The covariance function parameters $\Theta = \{\ell_1, \ldots, \ell_d, \eta^2\}$, which are usually called hyperparameters in machine learning, uniquely determine the GP surrogate model. In the Bayesian context, it is common practice to infer the hyperparameters by maximizing the

marginal likelihood of training data. In doing so, estimation of the hyperparameters is converted in an optimization problem of minimizing the negative logarithmic marginal likelihood (NLML). With a Gaussian likelihood, the NLML $\mathrm{L}(\boldsymbol{\Theta})$ and its partial derivatives are [44]

$$\mathrm{L}(\boldsymbol{\Theta}) = \frac{1}{2}\mathbf{S}^{\cdot}\,\mathbf{C}^{-1}\mathbf{S} + \frac{1}{2}\log|\mathbf{C}| + \frac{n}{2}\log(2\pi) \tag{15}$$

$$\frac{\partial \mathrm{L}(\boldsymbol{\Theta})}{\partial \Theta_i} = \frac{1}{2}\mathrm{tr}\left(\mathbf{C}^{-1}\frac{\partial \mathbf{C}}{\partial \Theta_i}\right) - \frac{1}{2}\mathbf{S}^{\cdot}\,\mathbf{C}^{-1}\frac{\partial \mathbf{C}}{\partial \Theta_i}\mathbf{C}^{-1}\mathbf{S} \tag{16}$$

where $|\bullet|$, $\mathrm{tr}(\bullet)$, and $(\bullet)^{\cdot}$ represent the determinant, trace, and transpose operators, respectively.

## 2.3 Uncertainty quantification of seismic performance

With respect to the seismic performance of PSWS, the uncertainty in structural parameter can be characterized by the probability density function (PDF), and the induced uncertainty of seismic responses is characterized in terms of statistics: mean and variance. Since $s(\mathbf{x})$ follows a Gaussian distribution with mean $\mu_s$ and variance $\sigma_s^2$ given in Equations (13) and (14), the expressions of statistics are

$$\mathrm{E}\left(s(\mathbf{x})\right) = \int \mu_s p(\mathbf{x}) d\mathbf{x} \tag{17}$$

$$\mathrm{V}\left(s(\mathbf{x})\right) = \int \left(\sigma_s^2 + \mu_s^2\right) p(\mathbf{x}) d\mathbf{x} - \left(\int \mu_s p(\mathbf{x}) d\mathbf{x}\right)^2 \tag{18}$$

where $\mathrm{E}(\bullet)$ and $\mathrm{V}(\bullet)$ represents the expectation and variance operators, respectively.

Using the separability of the covariance function, Equations (13) and (14) can be rearranged in a separate form [45]

$$\mu_s = c\sum_{i=1}^{n}\boldsymbol{\alpha}_i\prod_{k=1}^{d}N_{x_k}\left(x_k^i, \ell_k^2\right) \tag{19}$$

$$\sigma_s^2 = \eta^2 - c^2\sum_{j=1}^{n}\sum_{i=1}^{n}\mathbf{C}_{ij}^{-1}\prod_{k=1}^{d}N_{x_k}\left(x_k^i, \ell_k^2\right)N_{x_k}\left(x_k^j, \ell_k^2\right). \tag{20}$$

where $c = \eta^2(2\pi)^2\prod_{k=1}^{d}\ell_k$; $\mathbf{C}_{ij}^{-1}$ is the $(i,j)$-element of $\mathbf{C}^{-1}$; $x_k$ denotes the $k$-th parameter of $\mathbf{x}$; and $x_k^{i/j}$ represents the $(i/j,k)$-element of the input component of

training data $\mathbf{X}$. Substitution of Equations (19) and (20) into Equations (17) and (18), yields

$$\mathrm{E}\left(s(\mathbf{x})\right) = c\sum_{i=1}^{n}\boldsymbol{\alpha}_i\prod_{k=1}^{d}I_k^i \tag{21}$$

$$\mathrm{V}\left(s(\mathbf{x})\right) = \eta^2 + c^2\sum_{j=1}^{n}\sum_{i=1}^{n}\left(\boldsymbol{\alpha}_i\boldsymbol{\alpha}_j - \mathbf{C}_{ij}^{-1}\right)\prod_{k=1}^{d}\mathrm{N}_{x_k^i}\left(x_k^j, 2\ell_k^2\right)I_k^{ij} - \left(c\sum_{i=1}^{n}\boldsymbol{\alpha}_i\prod_{k=1}^{d}I_k^i\right)^2 \tag{22}$$

where $I_k^i, I_k^j, I_k^{ij}$ are single-dimensional integrals [45]. As indicated, the complicated high-dimensional integrals associated with mean and variance are successfully decomposed into the simple one-dimensional integrals.

### 2.4 Implementation summary

The GP surrogate model-based methodology is adopted to efficiently compute the statistics of seismic responses of PSWS. The methodology for uncertainty quantification of seismic response consists of two main procedures: (I) Sobol sequence, a space-fill experimental design, is used to create input component of training data. Then nonlinear seismic response analysis of PSWS is carried out at each sample point to obtain the corresponding seismic responses; and finally, GP surrogate model which characterizes the input-output relationship is built based on the training data. (II) Scenario-based assessment of seismic responses of PSWS is preformed within GP surrogate model framework; due to the use of surrogate model, the high-dimensional integrals associated with statistics (mean and variance) of seismic responses of PSWS can be successfully decomposed into one-dimensional integrals, which makes the task of uncertainty quantification of seismic response computationally efficient. The implementation of the developed probabilistic approach for seismic performance assessment of PSWS is detailed in Table 1.

## 3 FE modeling of the wharf structures

### 3.1 Description of the wharf structure

The target structure, as shown in Figure 1, is a typical pile-supported container wharf, which is 317 m long and 30.5 m wide. Such wharf structure is located at port of Los Angeles

Berth 100. Detailed information of this wharf is found in the references [13, 46]. Along the longitudinal direction, there are a total of 52 bays with an identical interval of 6.1 m. Along the transverse direction, there exist six rows of pre-stressing concrete piles with an octagonal shape and each side is around 0.253 m long. In particular, the distance between the pile row 1 and 2 is 3.7m, and the remaining pile row distances are 6.7 m. Each pile has a length of 42 m, and the pile rows 1 and 2 have 2.2 m long segment above the ground. The concrete deck supported on these octagonal-shaped piles has a least thickness of 0.4 m. The depth of the soil layers at the landside and waterside are 53.8 m and 33.5 m, respectively. The dike that aims to enhance the stability of PSWS has an inclination of 31 degree. The water level is located on the top of loose marine sand. The configuration details of the wharf structure are show in Figure 2.

### 3.2 FE modeling

Various types of elements are used to model the pile-supported wharf-ground system. This constructed FE model has 1393 nodes and 1305 elements, including 1186 soil elements and 119 nonlinear beam-column elements. It is worth to mention that the numerical model employs a high permeability (i.e., 1 m/s) as the liquefaction is not a main problem considering the relatively high friction angle for sand stratum. The resulting FE model of the PSWS is shown in Figure 3. The modeling details of the pile-supported wharf-ground system are given subsequently.

#### 3.2.1 Modeling of soil domain

The whole soil domain is idealized into four units including 9 sub-layers as well as the dike structure, where different colors represent different soil layers. The properties of soil stratum are displayed in Table 2. The saturated soil is modeled using 2D four-node plane-strain bilinear isoparametric elements. Such element is able to characterize the dynamic behavior of two-phase solid-fluid fully coupled material [47]. Each node of this element has

three degree-of-freedoms (DOFs), where DOFs 1 and 2 are used to represent the solid displacement and DOF 3 is used to represent the fluid pressure. The water is modeled by applying the hydrostatic pressure on the ground surface at the waterside. Meanwhile, to calculate the effective stresses correctly on the soil layer, the average nodal loads caused by the water weight above the soil surface is also considered in this FE model [48]. Note that in the real situation, the soil stratum has the stress and pore pressure fields but with zero displacement field under the soil gravity. The OpenSees computer program is able to ensure the zero displacement of model in the gravity phase [49]. To this purpose, two gravity runs need to be performed: 1st gravity run with activating the initial state analysis feature to obtain non-zero stress, pore pressure, and displacement fields; and 2nd gravity run with deactivating this feature to achieve the zero displacement field while maintaining stress and pore pressure field.

### 3.2.2 Modeling of the wharf structure

The pile geometry section and the fiber discretization of pile cross section are shown in Figure 4(a) and (b), respectively. The nonlinear properties of prestressed reinforced concrete pile are approximately modeled based on the fiber section with Kent-Scott-Park concrete model [50] and Giuffre-Menegotto-Pinto steel model [51]. The properties of concrete and steel in fiber section are listed in Table 3. Figure 4(c) illustrates the moment-curvature response of prestressed concrete pile with different axial forces.

The wharf deck is modeled using elastic beam element. In order to capture the skin-friction mechanism in the interface of soil and pile, the yield shear force of this mechanism is defined. The schematic soil-pile interface connection is presented in Figure 5. Two additional nodes between soil and pile nodes are added to connect the elastic beam and zero-length element (Figure 5(b)), which enforce the same DOF between the connected two nodes. This connection is created by the equal DOF constraint, zero-length element, and

elastic beam. Herein, the zero-length element provides the yield shear force, perpendicular to the axial force to simulate the slip at the soil-pile interface. The yield shear force of soil-pile interface comes from two parts: one part related to cohesion and the other part related to friction. The cohesion component is defined as [13]

$$F_{\text{cohesion}} = l \times h \times c \tag{17}$$

where $l$ is the pile perimeter; $h$ is the distance of center to center for the adjacent pile element; -and $c$ is the soil cohesion. The friction component is expressed as [13]

$$F_{\text{friction}} = \sigma_v \times \frac{\nu}{1-\nu} \times l \times h \times \tan\phi \tag{18}$$

where $\sigma_v$ is the vertical stress; $\nu$ is the Possion's ratio; and $\phi$ is the friction angle. Noted that $\sigma_v$ should be the vertical effective stress for saturated case. According to the summation of yield shear force and number of zero-length element along the pile perimeter, the yield shear force of every element can be computed.

### 3.2.3 Boundary and loading conditions

To ensure free-field conditions, lateral boundary is applied by employing the larger soil column to simulate the effect of free field boundary (Figure 6). Other boundary conditions imposed on the model are: (I) the nodes at the bottom of the model are fixed in all directions before shaking, and the lateral displacement in the shaking direction is left free until the base excitations are inputted into the model; (II) the nodal pore pressure is specified on the ground surface at the waterside according to the water height, that is, the ground surface boundaries at the waterside and landside are pervious; and (III) both lateral boundaries are impervious, so the pore pressure DOFs of the nodes at both lateral boundaries are also impervious.

Both linear and nonlinear analyses are performed for the wharf-ground system. In a linear analysis, a gravity application analysis (self-weight modeling) is performed before seismic excitation. After that, the initial state analysis is carried out to maintain the soil stress states and make the soil displacement zero through the OpenSees

InitialStateAnalysisWrapper [49]. The resulting soil stress states serve as initial conditions for the subsequent dynamic analysis. In the whole analysis, 5 runs are conducted in sequence in order to achieve convergence and simulate the actual loading situation. For the 1st run, the gravity is applied and nodal force and pore pressure loads on the ground surface at the waterside are applied; for the 2nd run, all elements keep the same properties as those in the 1st run and the initial state analysis is employed to ensure that the soil has non-zero stress and strain with zero displacement; for the 3rd run, the pile and soil-pile link element (i.e., zero-length element) are added to keep the same properties as those in the 2nd run; for the 4th run, only the soil properties are changed from elastic to plastic, and the remaining properties keep the same properties as those in the 3rd run; finally, for the 5th run, all materials keep the same properties as those in the 4th run and dynamic excitation is applied. This acceleration is generated from the 1994 Northridge earthquake ground surface Rinaldi Receiving Station record (Component S48W) and is scaled down to the amplitude of 0.22 g considering the effect of depth and soil property, as shown in Figure 7.

## 4 Scenario-based seismic assessment of PSWS

### 4.1 Seismic performance indicators and parameter characteristics

For the PSWS under consideration, the seismic responses associated with different structural components (namely, wharf deck, slope, and pile) are investigated. Particularly, the seismic responses under investigation are the maximum displacement of the concrete deck ($D_{\mathrm{max,deck}}$), the maximum displacement on the middle of the slope ($D_{\mathrm{max,dike}}$), and the maximum axial force ($F_{\mathrm{max,top}}$) and bending moment ($M_{\mathrm{max,top}}$) on the top of pile row 1. These four seismic responses are selected for the subsequent seismic analysis.

The random variables within the computational process are shown in Table 4. To have a visualization of the variability in seismic responses induced by the parameter uncertainty, the

time-history seismic responses corresponding to 300 parameter samples, which are generated based on Sobol sequence [39], are shown in Figures 8. More specifically, Figure 8(a) shows that the deck displacement at the end of shaking is about 38 cm and the displacement is accumulated mainly during the 2.5-6 s time interval due to the large acceleration pulse. Figure 8(b) indicates that the slope displacement shows a similar development pattern as the deck displacement, but its magnitude is smaller. As shown in Figure 8(c), the observed non-zero axial force at the beginning of shaking is due to self-gravity of deck; and the maximum axial force on pile top occurs at about 2.5 s, which corresponds to the peak acceleration (Figure 7). Figure 8(d) displays that the bending moment is almost zero at the begin of shaking, which means that the bending moment is mainly caused by seismic excitation. It is important to note that the nonzero axial force at end of shaking is due to the self-gravity of deck and the residual displacement caused by the large acceleration pulse, while the bending moment is nonzero owing to the residual displacement only. Overall, Figure 8 reveals to some extent that the parameter uncertainty will lead to the variation of seismic responses and the response variability becomes larger with the increase in the parameter uncertainty level. Probabilistic assessment of structural seismic responses using the developed GP surrogate model-based approach is discussed subsequently.

**4.2 Investigation of computational efficiency and accuracy**

The feasibility of the GP surrogate model-based approach in assessment of seismic responses is demonstrated using brute-force MCS. All tasks, including nonlinear seismic response analysis and surrogate modeling, are performed on a ThinkStation P700 desktop with Dual Intel Core i7-7700K processor and 16 GB memory. Combined with the parallel machine, the Single Parallel OpenSees Interpreter (called OpenSeesSP), which is widely applied to perform analysis of very large models, is utilized herein for increasing the computational efficiency.

Following the implementation procedures for the GP surrogate model-based method detailed in Table 1, the statistics of seismic responses of PSWS can be evaluated. On the other hand, MCS, which is widely used as the reference of other probabilistic approaches because of its generality, stability, and easy implementation, is also adopted to compute the statistics. A large sample size of 60,000 is used in order to ensure the convergence of sample statistics. The statistics of seismic responses of PSWS obtained by the GP surrogate model-based method and MCS are summarized in Table 5, where the associated computational costs are also provided. As shown in Table 5, the GP surrogate model-derived statistics are in close agreement with the MCS-derived ones. In particular, the largest relative errors of mean and standard deviation are 0.0407% and 3.2767%, respectively. The slight discrepancy between the GP surrogate model- and MCS-derived results demonstrates that the present GP surrogate model-based approach is effective and reliable for probabilistic assessment of seismic performance by considering the uncertainties associated with structural parameters. In addition to the accuracy of the present method, its computational efficiency is also of concern. As seen in the last row of Table 5, the total computational expense of generating training data and GP surrogate modeling is 586.4 min (around 9.7 hours). Specifically, the computational cost associated with GP surrogate modeling alone is only 11.4 min, and the remaining 575 min are accounted for by performing the nonlinear seismic response analysis for creating training data. In contrast, the brute-force MCS takes 115,000 min. In terms of the computational time, the GP surrogate model-based method exhibits overwhelming superiority over the brute-force MCS. Accordingly, it can be concluded that the proposed method is effective and computationally efficient for uncertainty quantification of seismic response.

### 4.3 Probabilistic assessment of seismic responses considering uncertainties of structural parameters

To explore how the parameter uncertainty level, measured by coefficient of variation (COV), influences the uncertainty of the seismic responses, a total of six COV scenarios are considered, that is, 5%, 10%, 15%, 20%, 25%, and 30%. The results are shown in Figure 9, which is an error bar plot with mean ($\mu$) plus/minus one standard deviation ($\sigma$). To further see how the variability of seismic responses is affected by parameter uncertainty size, the relationship between the COVs of seismic responses and the COVs of structural parameters is depicted, as shown in Figure 10. From the results of probabilistic seismic response assessment shown in Figures 9 and 10, several observations can be made.

As shown in Figure 9, the expected values of seismic responses of PSWS remain stable with the increase in COVs of structural parameters. This reveals that each of these 4 seismic responses has relatively a steady level over the different ranges of parameter values. It should be noted that this phenomenon may not be observed when the definition of parameter uncertainty is different. The standard deviations rise with the increase in COVs of structural parameters, which means that although the wider range of parameter variation does not cause the obvious variation to the response means, it leads to the upsurge in the standard deviation of responses (that is, larger response variability). As shown in Figure 10, an increase in COVs of structural parameters leads to an increase in COVs of all seismic responses.

## 5 Conclusions

This paper focuses on scenario-based seismic performance of PSWS considering parameter uncertainty. In this study, a fast-to-run GP surrogate model, which is a nonparametric and probabilistic model formulated from a Bayesian setting, is adopted to replace the computationally demanding FE model. The subsequent uncertainty quantification of seismic response is conducted exclusively within the framework of GP surrogate model. Specifically, this model is used to compute two order statistics (i.e., mean and variance) of seismic responses of PSWS. The limitation of high computational cost involved in

uncertainty quantification of seismic response of PSWS is overcome by the proposed surrogate modeling approach.

This approach is employed for uncertainty quantification of the interested seismic responses of PSWS with the defined uncertain structural parameters. On the other hand, the brute-force MCS is used as the reference solution for verification purpose. The excellent agreement between the GP surrogated model- and MCS-derived seismic response statistics verifies the high accuracy of the present approach. In particular, the largest relative errors of mean and standard deviation are 0.0407% and 3.2767%, respectively. In terms of the computational cost, the GP surrogate model-based approach maintains overwhelming superiority over the brute-force MCS. To be specific, the former takes 9.7 hours in total and the computational time associated with GP surrogate modeling alone is only 11.4 min, whereas the latter takes around 115,000 min. Therefore, the proposed GP surrogate model-based methodology holds high computational accuracy and efficiency in uncertainty quantification of seismic response of a large-scale PSWS. The results obtained by the GP surrogate modeling approach enable modelers to gain insight into the effects of uncertain structural parameters on the seismic performance of PSWS.

**Acknowledgements**

This research was financially supported by the Special Project Fund of Taishan Scholars of Shandong Province, China (No. 2015-212) and the Shandong Provincial Natural Science Foundation, China (No. ZR2017QEE007). The second author would like to appreciate the funding support by the Hong Kong Scholars Program (Grant No. XJ2016039).

**References**

[1] Na UJ, Chaudhuri SR, Shinozuka M. Probabilistic assessment for seismic performance of port structures. Soil Dynamics and Earthquake Engineering 2008; 28(2):147-158.

[2] Mylonakis G, Syngros C, Gazetas G, Tazoh T. The role of soil in the collapse of 18 piers of Hanshin Expressway in the Kobe earthquake. Earthquake engineering & Structural Dynamics 2006; 35(5):547-575.

[3] Werner SD, Dickenson SE, Taylor CE. Seismic risk reduction at ports: Case studies and acceptable risk evaluation. Journal of Waterway, Port, Coastal, and Ocean Engineering 1997; 123(6):337-346.

[4] Chung RM. The January 17, 1995 Hyōgo-ken-Nanbu (Kobe) Earthquake: performance of structures, lifelines, and fire protection systems. US Department of Commerce, Technology Administration, National Institute of Standards and Technology, 1996.

[5] Green RA, Olson SM, Cox BR, Rix GJ, Rathje E, Bachhuber J, French J, Lasley S, Martin N. Geotechnical aspects of failures at Port-au-Prince Seaport during the 12 January 2010 Haiti Earthquake. Earthquake Spectra 2011; 27(S1):43-65.

[6] Takahashi A, Takemura J. Liquefaction-induced large displacement of pile-supported wharf. Soil Dynamics and Earthquake Engineering, 2005, 25(11):811-825.

[7] Roeder CW, Graff R, Soderstrom J, Yoo JH. Seismic performance of pile-wharf connections. Journal of Structural Engineering 2005; 131(3):428-437.

[8] Boroschek RL, Baesler H, Vega C. Experimental evaluation of the dynamic properties of a wharf structure. Engineering Structures 2011; 33(2):344-356.

[9] Blandon CA, Bell JK, Restrepo JI, Weismair M, Jaradat O, Yin P. Assessment of Seismic performance of two pile-deck wharf connections. Journal of Performance of Constructed Facilities 2010; 25(2):98-104.

[10] Shafieezadeh A, DesRoches R, Rix GJ, Werner SD. Seismic performance of pile-supported wharf structures considering soil-structure interaction in liquefied soil. Earthquake Spectra 2012; 28(2):729-757

[11] Shafieezadeh A, DesRoches R, Rix GJ, Werner SD. Three-dimensional wharf response to

far-field and impulsive near-field ground motions in liquefiable soils. Journal of Structural Engineering 2012; 139(8):1395-1407.

[12] Yang CSW, DesRoches R, Rix GJ. Numerical fragility analysis of vertical-pile-supported wharves in the western United States. Journal of Earthquake Engineering 2012; 16(4):579-594.

[13] Su L, Lu J, Elgamal A, Arulmoli AK. Seismic performance of a pile-supported wharf: Three-dimensional finite element simulation. Soil Dynamics and Earthquake Engineering 2017; 95:167-179.

[14] Schmuhl DT, Loos S, Hur J, Shafieezadeh A. Time-dependent probabilistic capacity degradation assessment of prestressed concrete piles in marine environment. Structure and Infrastructure Engineering 2018: 1-14.

[15] Rackwitz R. Reviewing probabilistic soils modelling. Computers and Geotechnics 2000; 26(3):199-223.

[16] Frangopol DM. Life-cycle performance, management, and optimisation of structural systems under uncertainty: accomplishments and challenges. Structure and Infrastructure Engineering 2011, 7(6): 389-413.

[17] Liel AB, Haselton CB, Deierlein GG, Baker JW. Incorporating modeling uncertainties in the assessment of seismic collapse risk of buildings. Structural Safety 2009; 31(2):197-211.

[18] Yazdani A, Nicknam A, Yousefi DE, Eftekhari SN. Entropy-based sensitivity analysis of global seismic demand of concrete structures. Engineering Structures 2017; 146:118-126.

[19] Celik OC, Ellingwood BR. Seismic fragilities for non-ductile reinforced concrete frames-Role of aleatoric and epistemic uncertainties. Structural Safety 2010; 32(1):1-12.

[20] Arshian AH, Morgenthal G, Narayanan S. Influence of modelling strategies on uncertainty propagation in the alternate path mechanism of reinforced concrete framed

structures. Engineering Structures 2016; 110:36-47.

[21] Vamvatsikos D, Fragiadakis M. Incremental dynamic analysis for estimating seismic performance sensitivity and uncertainty. Earthquake engineering & structural dynamics 2010; 39(2):141-63.

[22] Vancouver Tondelli M, Rota M, Penna A, Magenes G. Evaluation of uncertainties in the seismic assessment of existing masonry buildings. Journal of Earthquake Engineering 2012; 16(S1):36-64.

[23] Gokkaya BU, Baker JW, Deierlein GG. Quantifying the impacts of modeling uncertainties on the seismic drift demands and collapse risk of buildings with implications on seismic design checks. Earthquake Engineering & Structural Dynamics 2016; 45(10):1661-1683.

[24] Dong Y, Frangopol DM. Performance-based seismic assessment of conventional and base-isolated steel buildings including environmental impact and resilience. Earthquake Engineering & Structural Dynamics 2016; 45(5):739-756.

[25] Enright MP, Frangopol DM. Probabilistic analysis of resistance degradation of reinforced concrete bridge beams under corrosion. Engineering Structures 1998; 20(11):960-971.

[26] Tubaldi E, Barbato M, Dall'Asta A. Influence of model parameter uncertainty on seismic transverse response and vulnerability of steel-concrete composite bridges with dual load path. Journal of Structural Engineering 2011; 138(3):363-74.

[27] Nielson BG, DesRoches R. Analytical seismic fragility curves for typical bridges in the central and southeastern United States. Earthquake Spectra 2007; 23(3):615-633.

[28] Padgett JE, DesRoches R. Sensitivity of seismic response and fragility to parameter uncertainty. Journal of Structural Engineering 2007; 133(12):1710-1718.

[29] Nielson BG, DesRoches R. Seismic fragility methodology for highway bridges using a component level approach. Earthquake Engineering & Structural Dynamics 2007;

36(6):823-839.

[30] Dong Y, Frangopol DM, Saydam D. Time-variant sustainability assessment of seismically vulnerable bridges subjected to multiple hazards. Earthquake Engineering & Structural Dynamics 2013; 42(10):1451-1467.

[31] Dong Y, Frangopol DM. Risk and resilience assessment of bridges under mainshock and aftershocks incorporating uncertainties. Engineering Structures 2015; 83: 198-208.

[32] Zheng Y, Dong Y, Li Y. Resilience and life-cycle performance of smart bridges with shape memory alloy (SMA)-cable-based bearings. Construction and Building Materials 2018; 158:389-400.

[33] Bi K, Hao H, Chouw N. Required separation distance between decks and at abutments of a bridge crossing a canyon site to avoid seismic pounding. Earthquake Engineering & Structural Dynamics 2010; 39(3):303-323.

[34] Bi K, Hao H, Chouw N. Influence of ground motion spatial variation, site condition and SSI on the required separation distances of bridge structures to avoid seismic pounding. Earthquake Engineering & Structural Dynamics 2011; 40(9):1027-1043.

[35] Soleimani F, Vidakovic B, DesRoches R, Padgett J. Identification of the significant uncertain parameters in the seismic response of irregular bridges. Engineering Structures 2017; 141:356-372.

[36] Nour A, Slimani A, Laouami N, Afra H. Finite element model for the probabilistic seismic response of heterogeneous soil profile. Soil Dynamics and Earthquake Engineering 2003; 23(5):331-348.

[37] Mirfattah SA, Lai CG. Effect of uncertainties in soil properties on probabilistic seismic performance of pile-supported wharves. 6th International Conference on Earthquake Geotechnical Engineering, Christchurch, New Zealand; 2015.

[38] Heidary-Torkamani H, Bargi K, Amirabadi R. Seismic vulnerability assessment of

pile-supported wharves using fragility curves. Structure and Infrastructure Engineering 2014; 10(11):1417-1431.

[39] Heidary-Torkamani H, Bargi K, Amirabadi R, McCllough NJ. Fragility estimation and sensitivity analysis of an idealized pile-supported wharf with batter piles. Soil Dynamics and Earthquake Engineering 2014; 61:92-106.

[40] Simpson TW, Poplinski JD., Koch PN, Allen JK. Metamodels for computer-based engineering design: survey and recommendations. Engineering with computers, 2001, 17(2):129-150.

[41] Sobol IM. On the distribution of points in a cube and the approximate evaluation of integrals. USSR Computational Mathematics and Mathematical Physics 1967, 7(4): 86-112.

[42] Antonev I A, Saleev V M. An economic method of computing LPτ-sequences. USSR Computational Mathematics and Mathematical Physics, 1979, 19(1): 252-256.

[43] Wan HP, Ren WX. Parameter selection in finite-element-model updating by global sensitivity analysis using Gaussian process metamodel. Journal of Structural Engineering 2015; 141(6):04014164.

[44] Rasmussen CE, Williams CKI. Gaussian processes for machine learning. Cambridge: MIT press; 2006.

[45] Wan HP, Ren WX, Todd MD. An efficient metamodeling approach for uncertainty quantification of complex systems with arbitrary parameter probability distributions. International Journal for Numerical Methods in Engineering 2017; 109(5):739-760.

[46] EMI. Final geotechnical and seismic analyses and design report berth 100 container wharf, west basin Port of Los Angeles, San Pedro, California. Prepared by Earth Mechanics, Inc. (EMI) submitted to Port of Los Angeles, California, 2001.

[47] Yang Z, Elgamal A. Influence of permeability on liquefaction-induced shear deformation.

Journal of Engineering Mechanics 2002; 128(7):720-729.

[48] Vytiniotis A. Contributions to the analysis and mitigation of liquefaction in loose sand slopes. PhD thesis. Massachusetts Institute of Technology; 2011.

[49] McGann C, Arduino P, Mackenzie-Helnwein P. InitialStateAnalysisWrapper. http://opensees.berkeley.edu/wiki/index.php/InitialStateAnalysisWrapper; 2011.

[50] Mander JB, Priestley MJ, Park R. Theoretical stress-strain model for confined concrete. Journal of Structural Engineering 1988; 114(8):1804-1826.

[51] Filippou FC, Popov EP, Bertero VV. Effects of bond deterioration on hysteretic behavior of reinforced concrete joints. Report EERC 83-19. Earthquake Engineering Research Center, University of California, Berkeley, 1983.

[52] Blandon C. Seismic analysis and design of pile supported wharves. PhD Thesis, Rose School Pavia, 2007.

[53] Andrade JE, Borja RI. Quantifying sensitivity of local site response models to statistical variations in soil properties. Acta Geotechnica 2006; 1(1):3-14.

[54] Kayser M, Gajan S. Application of probabilistic methods to characterize soil variability and their effects on bearing capacity and settlement of shallow foundations: state of the art. International Journal of Geotechnical Engineering 2014; 8(4):352-364.

[55] Crespo-Minguillón C, Casas JR. Fatigue reliability analysis of prestressed concrete bridges. Journal of Structural Engineering 1998; 124(12):1458-1466.

[56] Biondini F, Bontempi F, Frangopol DM, Malerba PG. Reliability of material and geometrically non-linear reinforced and prestressed concrete structures. Computers & structures 2004; 82(13):1021-1031.

[57] Eldin MN, Kim J. Sensitivity analysis on seismic life-cycle cost of a fixed-steel offshore platform structure. Ocean Engineering 2016; 121:323-340.

Table 1. Scenario based seismic assessment of PSWS.

**Procedure1** *Formulation of GP surrogate model of PSWS*

1 Adopt Sobol sequence sampling scheme to generate $n$-set inputs $\mathbf{X}$ from structural parameters' probability distributions.

2 Conduct nonlinear seismic response analysis of PSWS at each set $\mathbf{x}_i$ of $\mathbf{X}$ to obtain the corresponding seismic response $s_i$

3 Organize training dataset $\mathrm{D}=[\mathbf{X},\mathbf{S}]$, where $\mathbf{X}=\{\mathbf{x}_1,\mathbf{x}_2,\ldots,\mathbf{x}_n\}$ and $\mathbf{S}=\{s_1,s_2,\ldots,s_n\}$.

Estimate the hyperparameters of GP surrogate model by solving the optimization problem defined below

4
$$\begin{cases}\boldsymbol{\Theta}=\arg\min\limits_{\boldsymbol{\Theta}}\mathrm{L}(\boldsymbol{\Theta})\\ \mathrm{L}(\boldsymbol{\Theta})=\dfrac{1}{2}\mathbf{S}^{\cdot}\mathbf{C}^{-1}\mathbf{S}+\dfrac{1}{2}\log|\mathbf{C}|+\dfrac{n}{2}\log(2\pi)\\ \dfrac{\partial\mathrm{L}(\boldsymbol{\Theta})}{\partial\boldsymbol{\Theta}_i}=\dfrac{1}{2}\mathrm{tr}\left(\mathbf{C}^{-1}\dfrac{\partial\mathbf{C}}{\partial\boldsymbol{\Theta}_i}\right)-\dfrac{1}{2}\mathbf{S}^{\cdot}\mathbf{C}^{-1}\dfrac{\partial\mathbf{C}}{\partial\boldsymbol{\Theta}_i}\mathbf{C}^{-1}\mathbf{S}\end{cases}$$

Characterize the relationship between seismic response of PSWS and structural parameters through GP surrogate model $s(\mathbf{x})$, which follows a normal distribution such that

5
$$\begin{cases}s(\mathbf{x})\sim\mathrm{N}\left(\mu_s,\sigma_s^2\right)\\ \mu_{s(\mathbf{x})}=\boldsymbol{\alpha}^{\cdot}\mathbf{C}_*\\ \sigma_{s(\mathbf{x})}^2=\tilde{C}-\mathbf{C}_*^{\cdot}\mathbf{C}^{-1}\mathbf{C}_*\end{cases}$$

**End procedure1**

**Procedure2** *Probabilistic assessment of structural seismic responses*

Expand the expressions of mean and variances as

1
$$\begin{cases}\mu_{s(\mathbf{x})}=c\sum\limits_{i=1}^{n}\boldsymbol{\alpha}_i\prod\limits_{k=1}^{d}N_{x_k}\left(x_k^i,\ell_k^2\right)\\ \sigma_{s(\mathbf{x})}^2=\eta^2-c^2\sum\limits_{j=1}^{n}\sum\limits_{i=1}^{n}\mathbf{C}_{ij}^{-1}\prod\limits_{k=1}^{d}N_{x_k}\left(x_k^i,\ell_k^2\right)N_{x_k}\left(x_k^j,\ell_k^2\right)\end{cases}$$

Evaluate the seismic response statistics based on the following formulae

2
$$\begin{cases}\mathrm{E}\left(s(\mathbf{x})\right)=c\sum\limits_{i=1}^{n}\boldsymbol{\alpha}_i\prod\limits_{k=1}^{d}I_k^i\\ \mathrm{V}\left(s(\mathbf{x})\right)=\eta^2+c^2\sum\limits_{j=1}^{n}\sum\limits_{i=1}^{n}\left(\boldsymbol{\alpha}_i\boldsymbol{\alpha}_j-\mathbf{C}_{ij}^{-1}\right)\prod\limits_{k=1}^{d}\mathrm{N}_{x_k^i}\left(x_k^j,2\ell_k^2\right)I_k^{ij}-\left(c\sum\limits_{i=1}^{n}\boldsymbol{\alpha}_i\prod\limits_{k=1}^{d}I_k^i\right)^2\end{cases}$$

3 Assess seismic response variability of PSWS via the obtained statistic information.

**End procedure2**

Table 2. Physical properties of soil under wharf structure [13, 43].

| Soil unit | | Elevation (m) | Soil description | Density, $\rho$ (kg/m$^3$) | Friction angle, $\varphi$ (°) | Shear modulus, $G$ (MPa) | Bulk modulus, $B$ (MPa) | Cohesion, $c$ (kPa) |
|---|---|---|---|---|---|---|---|---|
| I | | 52.0~54.2 | Sandy fill (above ground water table) | 1920 | | | | |
| II | A | 45.0~52.0 | Loose marine sand | 1920 | 32 | 100 | 469 | 0 |
| | B | 36.0~45.5 | Dense marine sand | 2000 | 36 | 151 | 703 | 0 |
| | C | 35.5~39.0 | Medium dense marine sand | 2000 | 34 | 127 | 591 | 0 |
| III | A | 29.5~37.0 | Soft to stiff lagoonal clay | 1760 | 0 | 26 | 122 | 80 |
| | B1 | 25.0~29.5 | Stiff lagoonal clay | 1840 | 0 | 43 | 200 | 108 |
| | B2 | 17.0~25.0 | Stiff lagoonal clay | 1840 | 0 | 84 | 391 | 135 |
| IV | A | 19.0~22.0 | Dense lakewood-San Pedro sand | 2000 | 36 | 186 | 868 | 0 |
| | B | 0~19.0 | Very dense lakewood-San Pedro sand | 2080 | 38 | 279 | 1300 | 0 |
| - | Dike | 32.0~52.0 | Quarry run | 2240 | 45 | 141 | 1363 | 20 |

Table 3. Properties of concrete and prestressing steel used in fiber section [13, 43, 49].

| Parameter | Description | Unit | Value |
|---|---|---|---|
| $f_c^{'}$ | Concrete compressive strength | MPa | -74.9 (-49.0) |
| $\varepsilon_c$ | Strain at concrete compressive strength | - | -0.005 (-0.002) |
| $f_{cu}$ | Concrete crushing strength | MPa | -63.0 (0) |
| $\varepsilon_{cu}$ | Strain at concrete crushing strength | - | -0.018 (-0.004) |
| $f_y$ | Steel yield strength, | MPa | 1490 |
| $E$ | Steel elastic modulus | MPa | $2.04\times10^5$ |
| $\sigma_{Init}$ | Prestressing | MPa | 1062 |
| $b$ | Steel strain-hardening ratio | - | 0 |

*Note*: the value outside parentheses represents the properties of confined concrete, while those inside parentheses characterize the properties of unconfined concrete.

Table 4. Uncertain parameters considered in PSWS.

| No | Parameter | Distribution | Mean (MPa) | COV (%) | Source |
|---|---|---|---|---|---|
| 1 | Shear modulus of loose marine sand (IIA) | Lognormal | 100 | 5,10,…,30 | Enright and Frangopol [25], Nour et al. [36], Andrade and Borja [53], Kayser and Gajan [54] |
| 2 | Shear modulus of dense marine sand (IIB) | Lognormal | 151 | | |
| 3 | Shear modulus of Medium dense marine sand (IIC) | Lognormal | 127 | | |
| 4 | Shear modulus of soft to stiff lagoonal clay (IIIA) | Lognormal | 26 | | |
| 5 | Shear modulus of stiff lagoonal clay (IIIB1) | Lognormal | 43 | | |
| 6 | Shear modulus of stiff lagoonal clay (IIIB2) | Lognormal | 84 | | |
| 7 | Shear modulus of dense lakewood-San Pedro sand (IVA) | Lognormal | 186 | | |
| 8 | Shear modulus of very dense lakewood-San Pedro sand (IVB) | Lognormal | 279 | | |
| 9 | Shear modulus of quarry run (Dike) | Lognormal | 141 | | |
| 10 | Compressive strength of confined concrete | Lognormal | -74.9 | 5,10,…,30 | Enright and Frangopol [25], Crespo-Minguillón et al. [55], Biondini et al. [56] |
| 11 | Compressive strength of unconfined concrete | Lognormal | -49.0 | | |
| 12 | Crushing strength of confined concrete | Lognormal | -63.0 | | |
| 13 | Yield strength of prestressing steel | Lognormal | 1490 | 5,10,…,30 | Eldin and Kim [57] |
| 14 | Elastic modulus of prestressing steel | Normal | $2.04\times10^5$ | | |
| 15 | Prestressing of steel | Lognormal | 1062 | 5,10,…,30 | Crespo-Minguillón et al. [55], Biondini et al. [56] |

*Note*: COV (coefficient of variation) is the ratio of the standard deviation to the mean.

Table 5. Comparison of computational accuracy and efficiency.

| | GP surrogate model | | MCS | | Relative error (%) | |
|---|---|---|---|---|---|---|
| | $\mu$ | $\sigma$ | $\mu$ | $\sigma$ | $\mu$ | $\sigma$ |
| $D_{max,deck}$ (cm) | 44.4780 | 0.2691 | 44.4660 | 0.2768 | 0.0270 | 2.7688 |
| $D_{max,dike}$ (cm) | 29.0675 | 0.2399 | 29.0794 | 0.2429 | 0.0407 | 1.2467 |
| $F_{max,top}$ (kN) | -944.5185 | 4.9393 | -944.3811 | 4.7826 | 0.0145 | 3.2767 |
| $M_{max,top}$ (kN-m) | 1193.7162 | 1.2913 | 1193.6700 | 1.2750 | 0.0039 | 1.2774 |
| Time (min) | 586.4 | | 115000 | | - | |

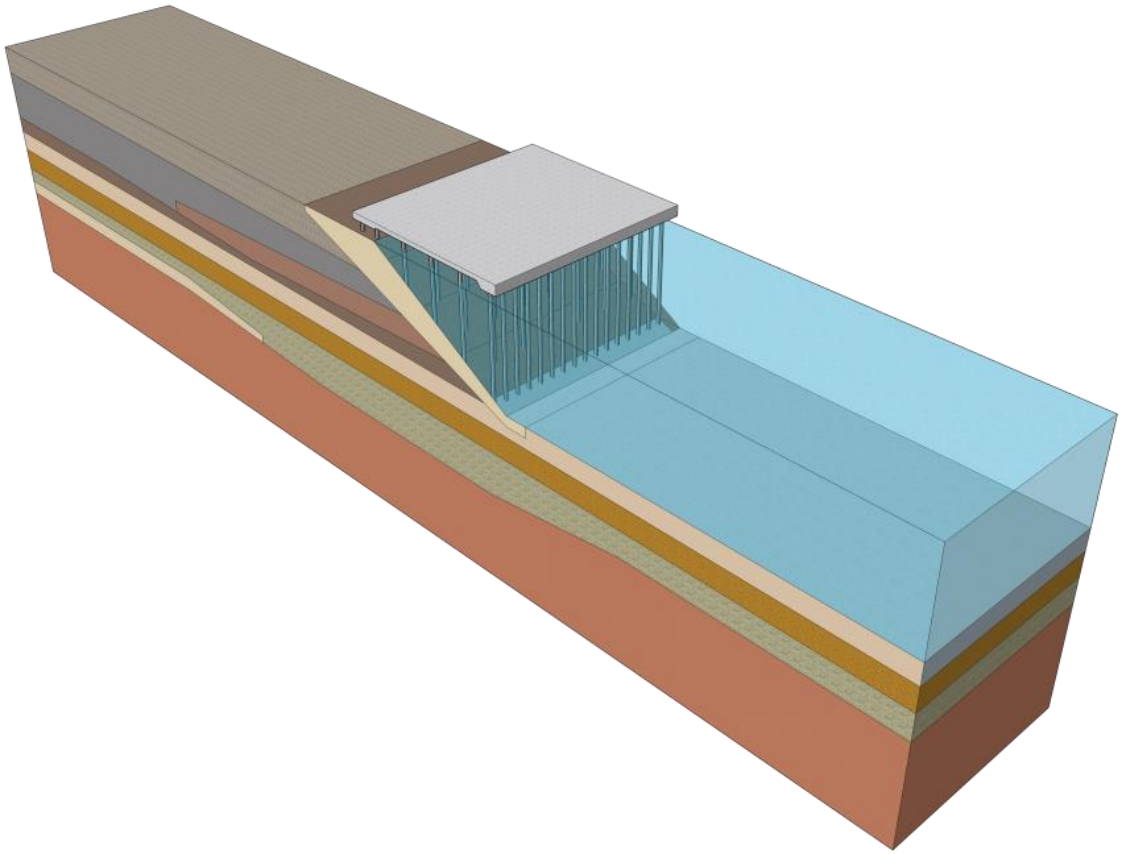

Figure 1. Three-dimensional view of pile-supported wharf structure.

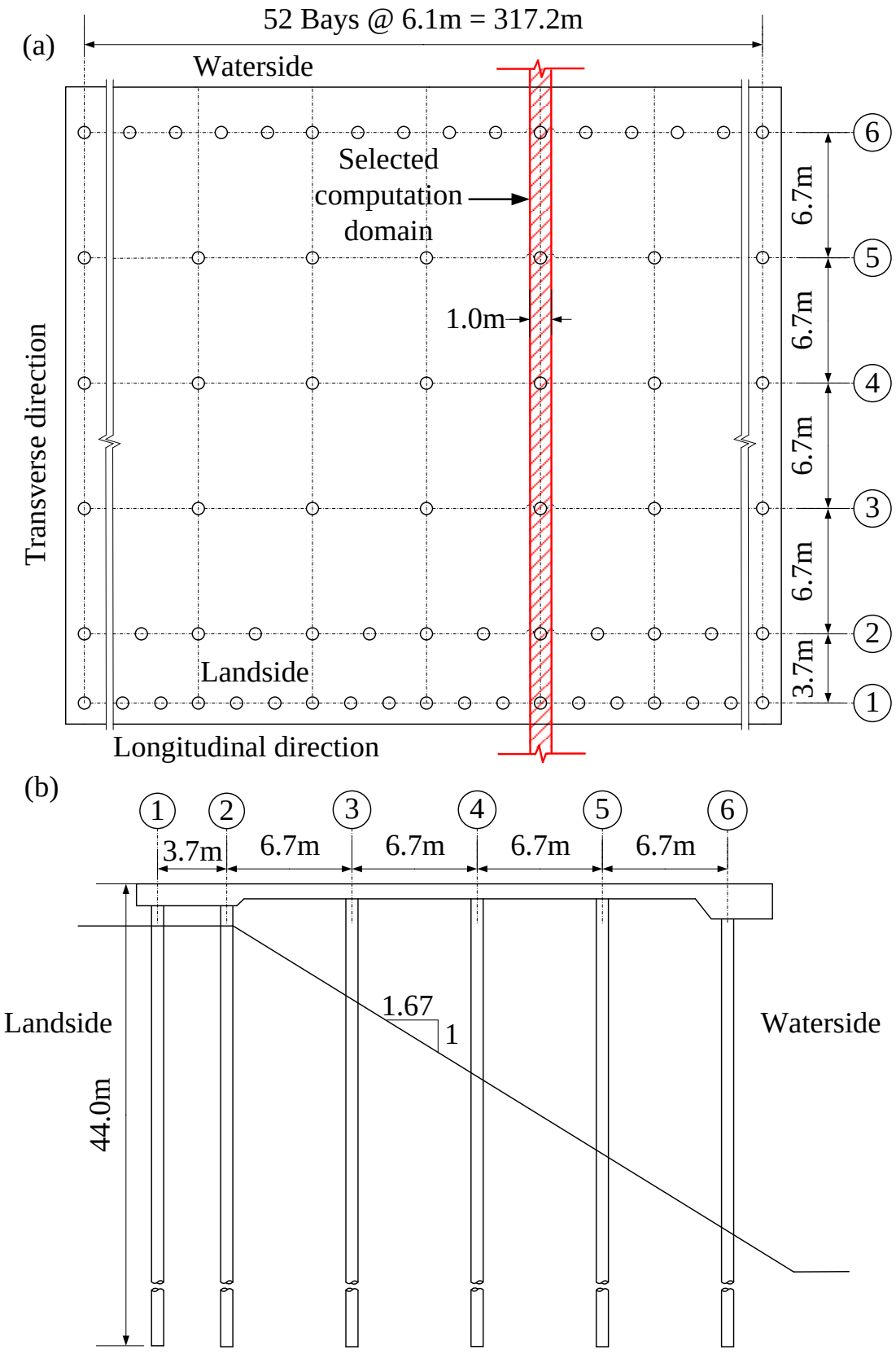


Figure 2. Configuration of wharf structure: (a) plan, and (b) elevation.

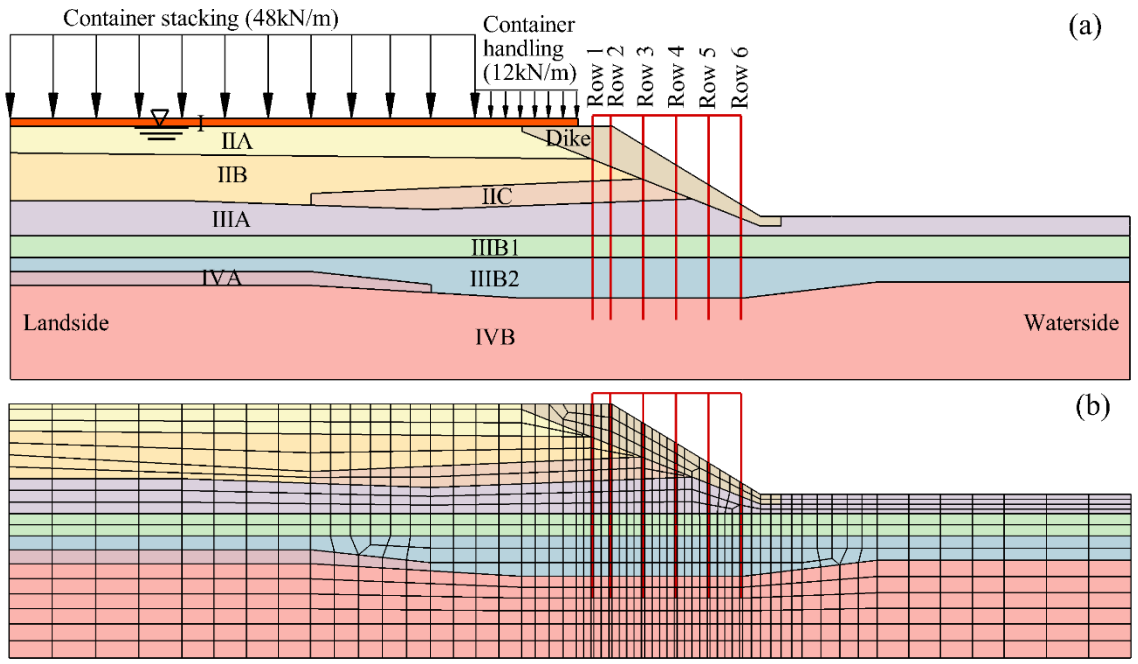


Figure 3. Pile-supported wharf structure: (a) model configuration, and (b) finite element mesh.

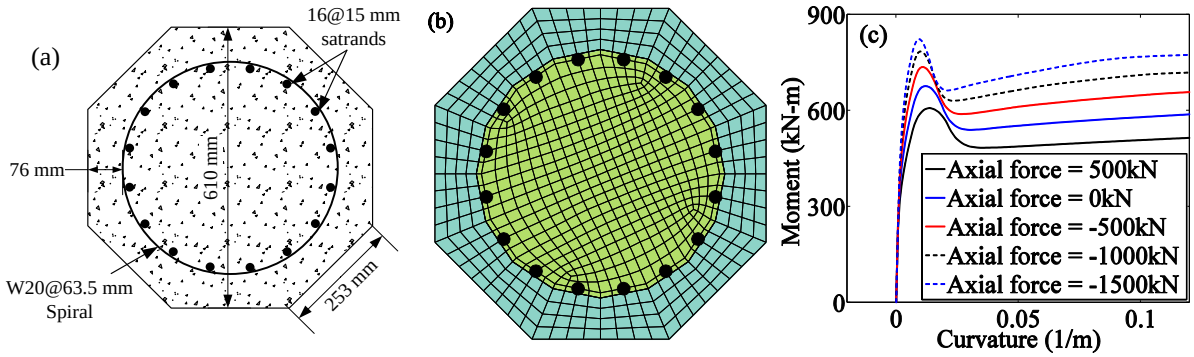


Figure 4. Configuration and moment-curvature response of pile: (a) pile geometry section, (b) fiber discretization of pile cross section, and (c) moment-curvature response under different axial forces

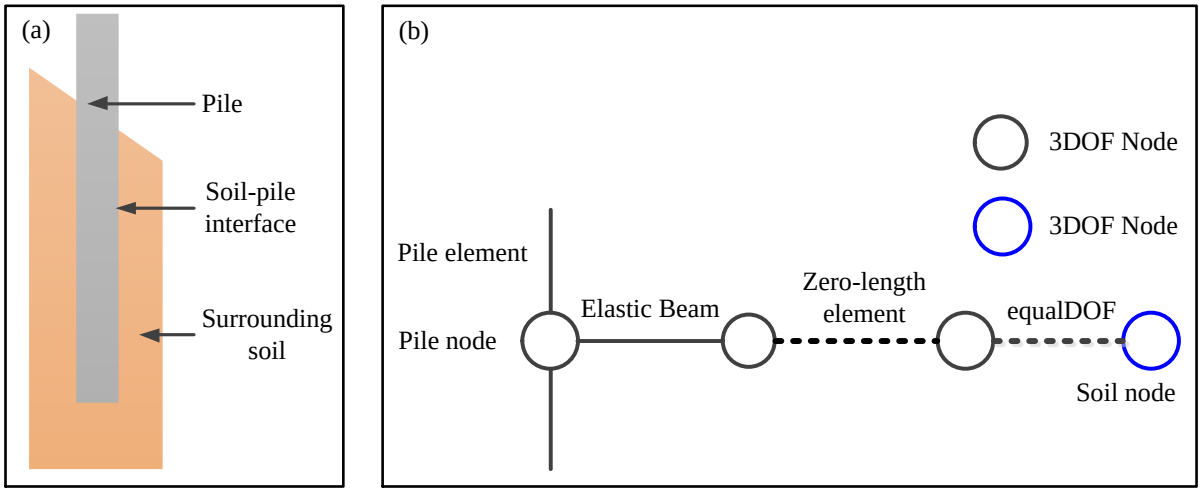


Figure 5. Soil-pile interaction modeling: (a) pile and surrounding soil, and (b) connection of soil-pile interface.

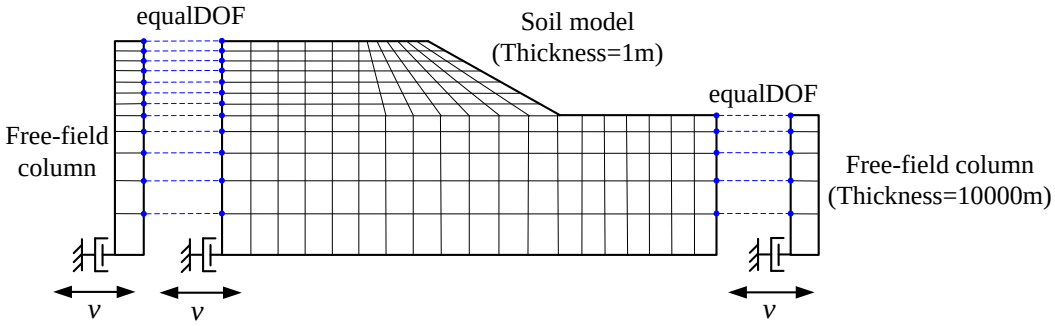


Figure 6. Lateral free-field boundary conditions and base excitation by velocity.

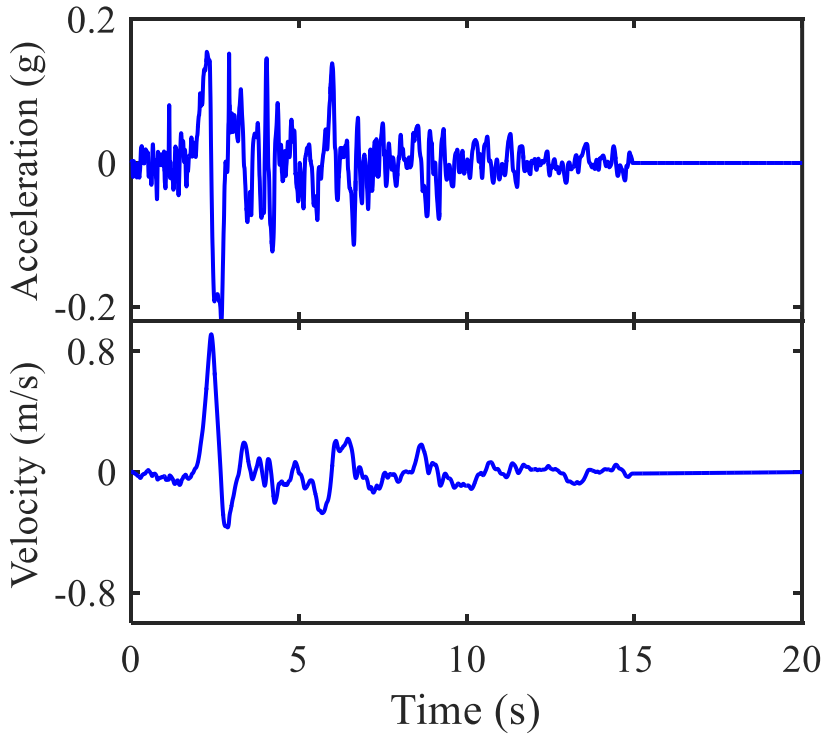


Figure 7. Base input acceleration and velocity time histories.

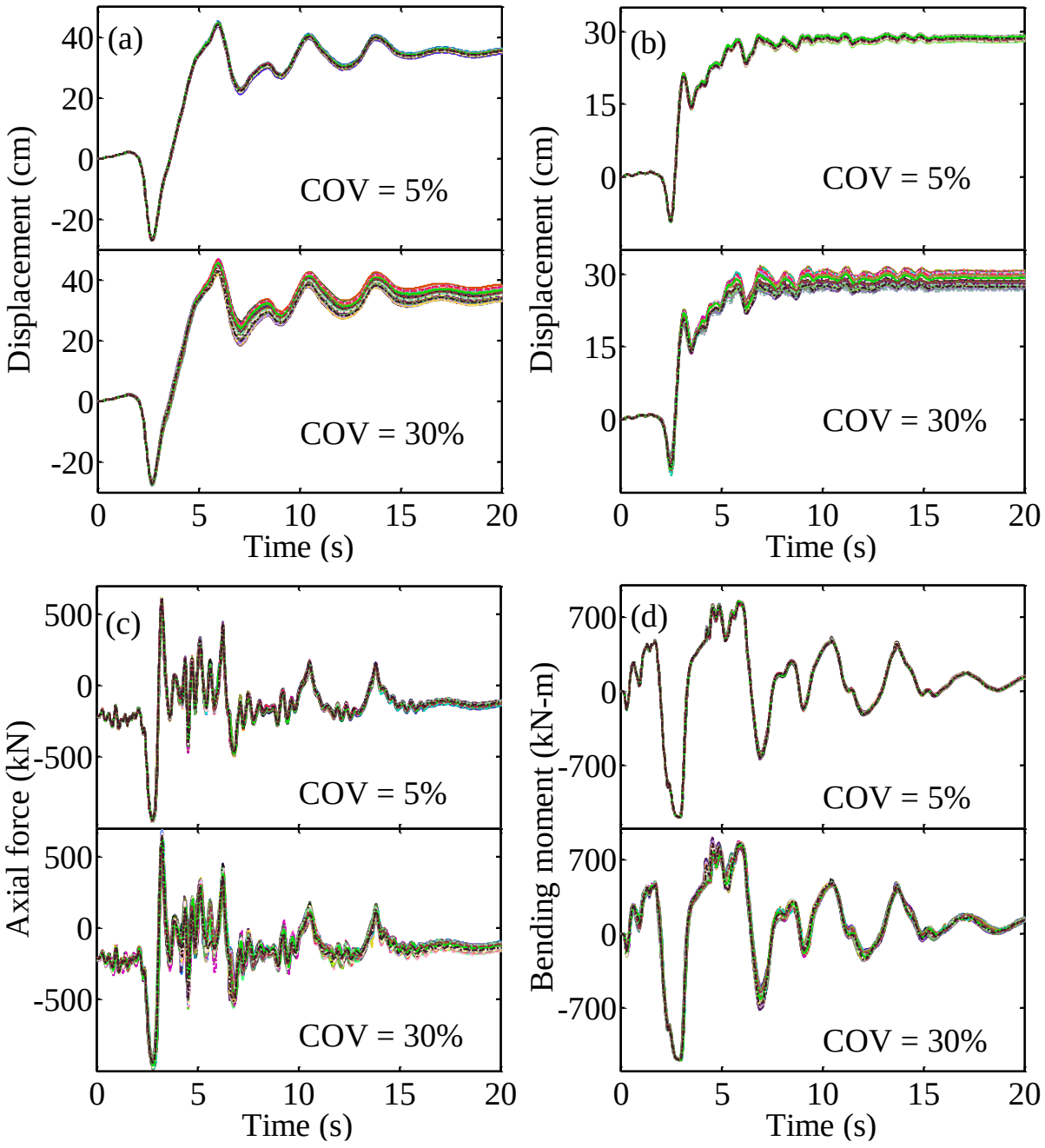


Figure 8. Seismic responses of wharf structure with different COVs of structural parameters: (a) deck displacement, (b) displacement on the middle of slope, (c) axial force on the top of pile row 1, and (d) bending moment on the top of pile row 1.

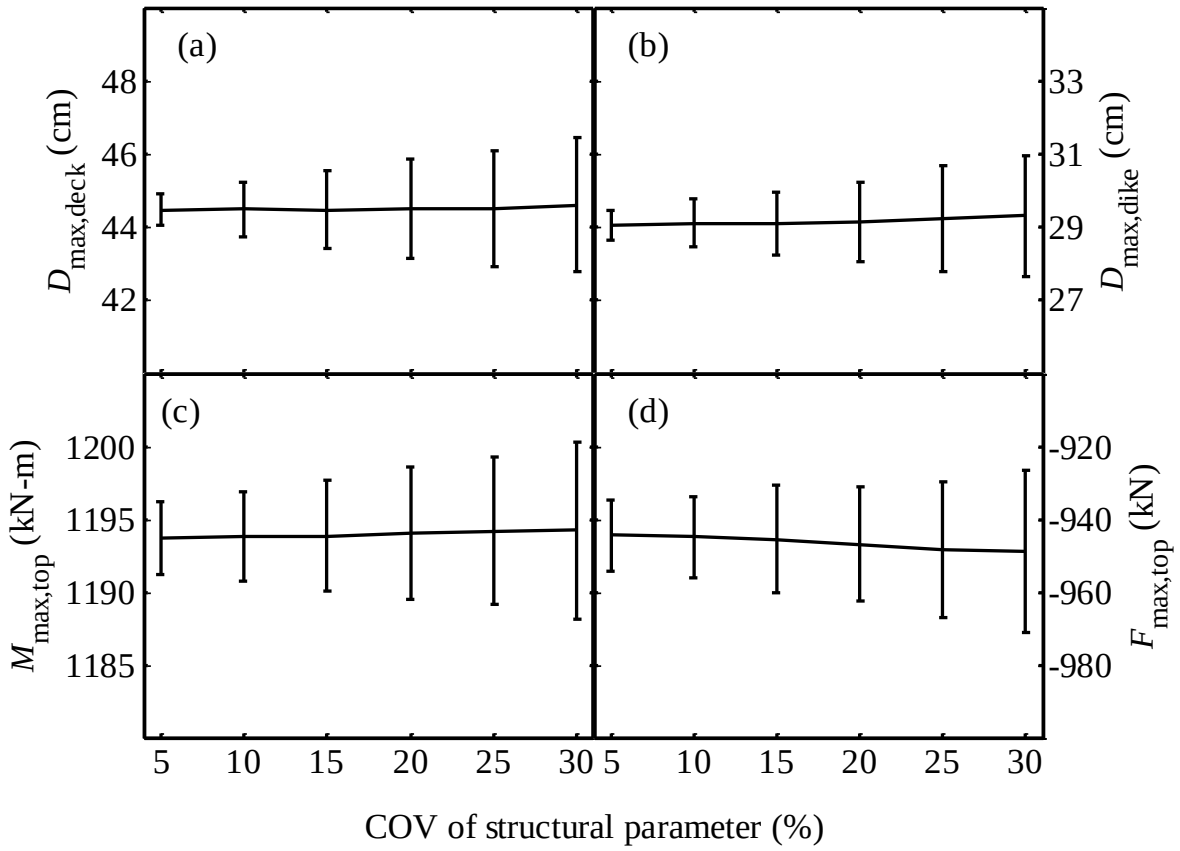


Figure 9. Statistics distribution of seismic responses of wharf structure under different parameter COVs: (a) deck displacement, (b) displacement on the middle of slope, (c) axial force on the top of pile row 1, and (d) bending moment on the top of pile row 1.

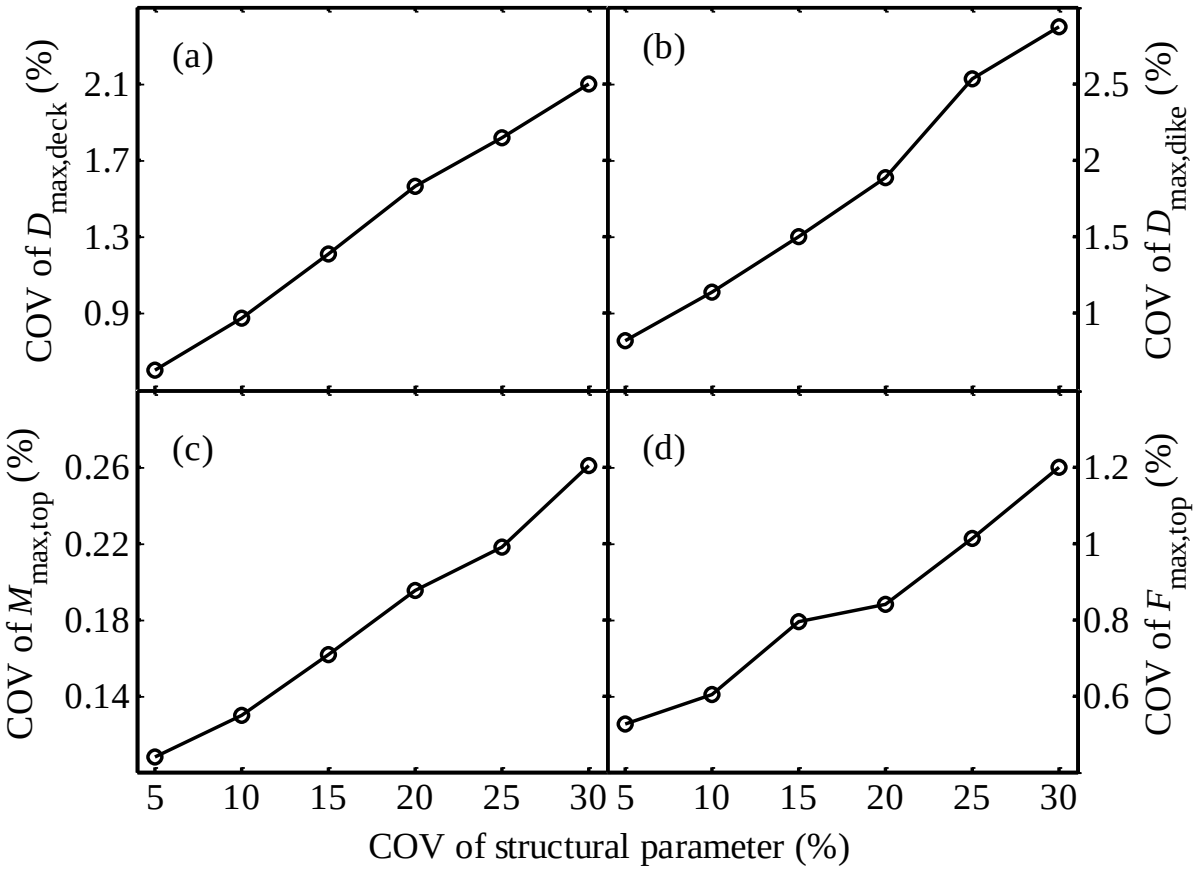


Figure 10. COV of seismic responses versus COV of structural parameters: (a) deck displacement, (b) displacement on the middle of slope, (c) axial force on the top of pile row 1, and (d) bending moment on the top of pile row 1.